Biomaterial Property Effects on Platelets and Macrophages: An in Vitro Study

Kelly R. Fernandes,[†,‡,§] Yang Zhang,[†,§] Angela M. P. Magri,[‡] Ana C. M. Renno,[‡] and Jeroen J. J. P. van den Beucken*,[†]

[†]Department of Biomaterials, Radboudumc, P.O. Box 9101, 6500HB Nijmegen, The Netherlands
[‡]Department of Biosciences, Federal University of São Paulo (UNIFESP), 136 Silva Jardim Street, Santos, SP 11015-021, Brazil

ABSTRACT: The purpose of this study was to evaluate the effects of surface properties of bone implants coated with hydroxyapatite (HA) and β-tricalcium phosphate (β-TCP) on platelets and macrophages upon implant installation and compare them to grit-blasted Ti and Thermanox used as a control. Surface properties were characterized using scanning electron microscopy, profilometry, crystallography, Fourier transform infrared spectroscopy, and coating stability. For platelets, platelet adherence and morphology were assessed. For macrophages, morphology, proliferation, and polarization were evaluated. Surface characterization showed similar roughness of ~2.5 μm for grit-blasted Ti discs, both with and without coating. Coating stability assessment showed substantial dissolution of HA and β-TCP coatings. Platelet adherence was significantly higher for grit-blasted Ti, Ti-HA, and Ti-β-TCP coatings compared to that of cell culture control Thermanox. Macrophage cultures revealed a decreased proliferation on both HA and β-TCP coated discs compared to both Thermanox and grit-blasted Ti. In contrast, secretion of pro-inflammatory cytokine TNF-α and anti-inflammatory cytokine TGF-β were marginal for grit-blasted Ti and Thermanox, while a coating-dependent increased secretion of pro- and anti-inflammatory cytokines was observed for HA and β-TCP coatings. The results demonstrated a significantly upregulated pro-inflammatory and anti-inflammatory cytokine secretion and marker gene expression of macrophages on HA and β-TCP coatings. Furthermore, HA induced an earlier M1 macrophage polarization but more M2 phenotype potency than β-TCP. In conclusion, our data showed that material surface affects the behaviors of first cell types attached to implants. Due to the demonstrated crucial roles of platelets and macrophages in bone healing and implant integration, this information will greatly aid the design of metallic implants for a higher rate of success in patients.
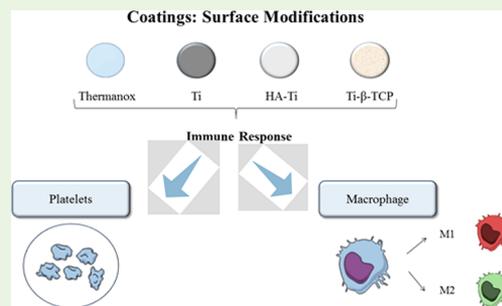
KEYWORDS: CaP coating, macrophage polarization, platelet activation, bone implants

1. INTRODUCTION

Implants for replacement and fixation after bony fractures have become a general treatment modality mainly in the current dental and orthopedic clinics, respectively. Generally, these bone implants are made from metallic materials that can withstand mechanical forces. Among the metallic materials used for bone implant preparation, titanium (Ti) presents excellent biocompatibility and high mechanical strength.[1,2] Also, from the biological perspective, orthopedic Ti implants can be improved by combining different surface modifications.[3] In view of this, research efforts have focused on the effect of surface modifications for implant surfaces to promote implant integration within the native bone tissue.[2,4−6]

The nature of these surface modifications can be categorized as either physical (e.g., roughness or topography) or chemical (e.g., coatings). In this way, titanium implants coated with different physiochemical properties can stimulate the osseointegration ability, directly affecting the performance and clinical success of the implant.[3] In this context, calcium phosphate ceramics (CaPs) are an appealing group of materials for the deposition of coatings for bone implants. Many studies have shown that CaP coatings, particularly those based on

hydroxyapatite (HA), β-tricalciumphosphate (β-TCP), or combinations thereof, provide a favorable microenvironment for the interaction of the implant surface with the bone tissue, allowing an accelerated and more effective integration of such implants in the surrounding bone tissue.[7−9]

Upon implantation, any biomaterial induces a cascade of events initiated by the activation of platelets and inflammatory cells (e.g., macrophages and foreign body giant cells).[10−13] Within this cascade of events, the challenge for the biomedical engineering field is to optimize the initial inflammatory events toward an effective regenerative phase and hence achieve an improved performance of biomedical devices.[10,14] In the initial inflammatory events, platelets play an active role in the immunological and inflammatory aspect of tissue healing in normal hemostasis as well as in host defense. Platelets can be directly involved in the inflammatory response by the production and release of several inflammatory mediators, including a variety of cytokines and chemokines.

Platelet activation results in stimulation of various leukocytes, including macrophages.[15] Beside platelets, macrophages also contribute to tissue homeostasis by clearance of injured host components and defense against infection. Once out of the circulation and in the tissue at a wounded site, macrophages can acquire different morphologies and functionalities in response to pathogens and local environmental stimuli. Two major macrophage subpopulations have been defined in vitro, designated as either classically activated macrophages (M1) or alternatively activated macrophages (M2).[16] Classically activated M1 induced by lipopolysaccharide (LPS), interferon (IFN)-γ, or tumor necrosis factor-α (TNF-α) are associated with the first phases of acute inflammation. This macrophage subtype is characterized by the secretion of pro-inflammatory cytokines, TNF-α, inducible nitric oxide synthase (iNOS or NOS2), reactive oxygen species (ROS), reactive nitrogen intermediates (RNI), promotion of Th1 responses, and strong microbicidal and tumoricidal activity.[17] In contrast, alternatively activated M2 macrophages are characterized by increased phagocytic activity, high expression of scavenging, mannose and galactose receptors, production of ornithine and polyamines through the arginase pathway, a distinct chemokine repertoire (e.g., CCL17, CCL18, and CCL22), and an IL-12^{lo}, IL-10^{hi}, IL-1, decoyR^{hi}IL, 1RA^{hi} phenotype.[18]

The role of implant surface properties in the initial phase after implantation is largely unknown. However, it is generally accepted that the physicochemical properties of a biomaterial surface (e.g., microporosity, surface roughness, coating chemistry, and solubility), the inflammatory response evoked in the tissue (i.e., platelet adhesion and activation and inflammatory responses), the design and size of the medical device, and the anatomical site in which it will be inserted[8,13,19] are major determinants for implant success. There is a vast amount of evidence that CaP biomaterials with osteogenic properties have enormous potential in bone healing, reducing the chances of complications and time to repair. Urquia Edreira et al.[20] evaluated the effect of CaP sputter-coatings with different phase composition in an in vitro and in vivo study. Their data demonstrated that the differences in physicochemical properties of the coatings affect both in vitro and in vivo results. One of the CaPs, the hydroxyapatite (HA), has been widely used to improve the bioactivity and osseointegration of metallic implants because it is an osteoconductive material capable of enhancing the bond with the surrounding bone tissue.[21] Several studies show positive effects on osseointegration of HA-coated metallic implants.[21–23] In addition, β-TCP is another widely used CaP that has osteoconductive properties to be used as a coating for Ti implants. Several studies demonstrated greater ability to form new bone after being implanted in the body.[24–26]

Although several studies have shown the effects of HA and TCP as coatings of metallic implants, the initial response of blood-born components (i.e., platelets and monocytes/macrophages) are largely neglected by many researchers evaluating bone response after implantation of a biomaterial. Consequently, we here evaluated biomaterial surface property effects on the response of blood-born components that account for the initial biological cascade of events following implantation. We used in vitro experiments with human platelets and monocytes/macrophages to investigate (i) platelet adhesion and (ii) monocyte/macrophage morphology, proliferation, cytokine secretion, and polarization using either unmodified or CaP-coated Ti discs. We hypothesized that CaP-coated discs (HA or β-TCP) would alter the initial response of blood-born components and platelet adhesion and macrophage secretion/polarization in favor of wound healing.

2. MATERIALS AND METHODS

2.1. Material Preparation and Characterization. Commercially available pure Ti discs (99.9 wt % Ti, thickness 1.5 mm, diameter 12 mm) were Al$_2$O$_3$ grit-blasted before deposition. The target materials used in the deposition process for the coating were hydroxyapatite (HA; Ca$_{10}$(PO$_4$)$_6$(OH)$_2$) granulated powder obtained from CAM-CERAM (CAM Bioceramics, Leiden, The Netherlands; low porous granules 500−1000 μm) and β-tricalcium phosphate (β-TCP; Ca$_3$(PO$_4$)$_2$) (CAM Bioceramics, Leiden, The Netherlands). The solubility product constants (K_{sp}) of HA and TCP are $10^{-116.8}$ and $10^{-28.9}$ mol/L, respectively. As a control, Ti discs and Thermanox coverslip (diameter: 13 mm; thickness: 0.2 mm; use with a 24-well multidish; Thermo Scientific Nunc) were used. The coatings for this study were deposited using RF magnetron sputtering equipment (Edwards High Vacuum ESM 100 system, Crawford, England) as described previously.[20,27−29] Before deposition, the discs were cleaned ultrasonically in acetone and propanol to remove impurities. Subsequently, the discs were placed on a rotating holder, and the coating deposition process with HA and β-TCP was initiated (sputtered target: HA and β-TCP; distance between target and implants: 80 mm; power: 400W; working gas: argon; pressure: 5.0 × 10^{-3}; treatment time: 10 h for HA deposition and 13 h for β-TCP deposition). After sputtering, the discs received a heat treatment of 15 s in air at final heating temperature of up to 600 °C using an infrared furnace (Quad Ellipse Chamber, Model E4- 10-P, Research, MN).[20] Infrared irradiation was carried out under pure argon flow as described by Yoshinari et al.[30]

2.2. Surface Analysis. Ti discs and HA and β-TCP coated discs were morphologically inspected by field emission scanning electron microscopy (FE-SEM; JEOL 6310, Nieuw-Vennep, The Netherlands). Additionally, thickness and roughness of the coatings (quadruplicate samples, $n = 4$) were measured using a Universal Surface Tester (UST, Würzburg, Germany).

2.3. Physicochemical Characterization and Stability of the Coatings. The crystal structure of each specimen was determined by X-ray diffraction (XRD, Phillips, PW3710, Eindhoven, The Netherlands) using Cu Kα radiation (power: 40 kV; current: 30 mA). In addition, infrared spectra of the coatings were obtained by a reflection Fourier transform infrared spectrometer (FTIR, PerkinElmer, Spectrum Two, Groningen, The Netherlands).

For analyzing coatings stability, discs (triplicate samples; $n = 3$) were placed in 4 mL of Milli-Q water and incubated at 37 °C in a water bath on a shaker Table (70 rpm) for 4 weeks. After 7, 14, 21, and 28 days of incubation, Milli-Q water was refreshed completely and used for the calcium assay based on orthocresolphtalein complexone (OCPC). At the end of the experimental period, the coated discs were incubated overnight in 1 mL of 0.5 N acetic acid on a shaker table to dissolve remaining calcium phosphate on the discs. For analysis, 300 μL of working reagent was added to 10 μL of sample or standard in a 96-well plate. The well plates were incubated for 10 min at room temperature. The absorbance was measured using a microplate spectrophotometer at 570 nm (Bio-Tech Instruments, Winooski, VT, United States). The total calcium content within the coatings (μg/cm^2) was determined by cumulating total calcium release and remaining calcium on the discs, normalized for disc surface area.

2.4. Platelet Experiments. Human platelet-rich plasma (hPRP) was obtained from Sanquin (Nijmegen, The Netherlands) with cell counts of $(4-5) \times 10^8$ platelets/mL. Platelets counts were obtained with a particle count and size analyzer according to the instructions of the manufacturer (Beckman Coulter, Z2, Florida, United States).

The experimental discs (quadruplicate samples; $n = 4$) were placed in 24-well plates with custom-made Teflon molds surrounding each disc and a cylindrical volume above the disc (1 mL volume) as described previously.[31] These molds restrict platelet adherence to only the disc surface. A platelet solution containing 200 μL of the freshly

Table 1. Primers and the Expected PCR Products Size for Each Gene Analyzed

gene	forward primer	reverse primer
human β-actina	CATCACCATTGGCAATGAGC	CGATCCACACGGAGTACTTG
INDO	CCTGAGGAGCTACCATCTGC	TCAGTGCCTCCAGTTCCTTT
CXCL11	AGTCCTGGAAAAGAGCATCT	TCACCCACCTTTCATCCTTC
MCR-1	GGTTTATGGAGCAGGTGGAA	AAACTTGAACGGGAATGCAC
CCL13	ATCTCCTTGCAGAGGCTGAA	ACTTCTCCTTTGGGTCAGCA

prepared PRP and EDTA solutions with a final concentration of 10 mm EDTA (Sigma, MO, United States) was added to each well containing one disc. Thereafter, the well plate was centrifuged at 150g for 10 min to achieve platelet adherence to the disc surface.

After centrifugation, the 24-well plates were incubated at 37 °C on a horizontal shaker (70 rpm) for 30 min. After that, the experimental discs were washed with PBS to remove nonadherent platelets and prepared for (qualitative) SEM examination of adherent platelets as well as (quantitative) lactate dehydrogenase (LDH) activity.

2.4.1. Scanning Electron Microscopy of Platelets. SEM (JEOL 6310, Nieuw-Vennep, The Netherlands) was used for qualitative analysis of adherent platelets. After 3 h of incubation, platelets were washed twice with PBS and subsequently fixed for 15 min in 2% glutaraldehyde in 0.1 M sodium cacodylate buffered solution. Then, samples were rinsed twice with cacodylate buffered solution and dehydrated using a graded series of ethanol. Finally, samples were dried with tetramethylsilane. The samples were sputter-coated with gold prior to SEM examination.

2.4.2. Platelet Adhesion. The quantification of platelet adherence was determined using a photospectrometric measurement based on kinetic determination of lactate dehydrogenase (LDH) activity.[7,32,33] Adherent platelets were lysed by adding 200 μL of 1% Triton buffer (Triton X-100, Sigma) to each well. The wells were incubated for 3 h at room temperature. After the incubation, 100 μL of each lysate was collected and mixed with 100 μL of reaction solution (LDH measurement kit, Roche Life Science, Almere, The Netherlands). Pursuant to the manufacturer's instructions, LDH activity was determined by recording absorbance at 490 nm.

2.5. Monocytes/Macrophage Experiments. The human monocytic cell line (THP-1; ATCC, LGC Standards GmbH, Germany) was cultured in Roswell Park Memorial Institute (RPMI) 1640 medium supplemented with 10% fetal bovine serum, 100 U/ml penicillin and streptomycin at 37 °C in a 5% CO_2 and 95% atmospheric air. THP-1 cells were activated into macrophages by 50 ng/mL phorbol-12-myristate-13-acetate (PMA) as previously reported.[34] Cells (1×10^5 cells/cm²) were seeded on the experimental discs in culture medium (quadruplicate samples; n = 4) and cultured for 1, 4, and 7 days.

2.5.1. Morphological Analysis. Cell morphology was assessed by SEM (JEOL 6310, Nieuw-Vennep, The Netherlands). After 1, 4, and 7 days, the cells were washed twice with PBS and subsequently fixed for 15 min in 2% glutaraldehyde in 0.1 M sodium cacodylate buffered solution. Then, samples were rinsed twice with cacodylate buffered solution and dehydrated using a graded series of ethanol. Finally, samples were dried with tetramethylsilane and sputter coated with gold prior to SEM analysis.

2.5.2. Cellular DNA Content. After day 1, 4, and 7 of cell culture, total DNA content was determined to obtain information about cellular proliferation. Cellular DNA content was measured using Quantifluor dsDNA System (Promega Benelux BV, Leiden, The Netherlands) according to the instructions of the manufacturer. Medium was removed; the cell layer was washed twice with PBS, after which 1 mL of Milli-Q was added to each well, and the samples were stored at −80 °C until further use. For the standard curve, serial dilutions of dsDNA stock were prepared to final concentrations of 0−2000 ng/mL. Next, 100 μL of each sample and 100 μL of freshly made 1× Quantifluor dye working solution were added to a 96-well plate in duplicate. The plates were incubated at room temperature in the dark for 5 min, after which the fluorescence excitation/emission at 480/520 nm was read.

2.5.3. Cytokine Measurements by ELISA. The secretion of TNF-α and transforming growth factor-β (TGF-β) was measured in the cell culture media. After 1, 4, and 7 days of culture, the culture medium was aspired and stored frozen at −80 °C until analysis. The concentrations of TNF-α (pro-inflammatory) and TGF-β (pro-wound healing) were determined using ELISA kits (Bioscience, United States) according to the manufacturer's instructions. Relative values of cytokine secretion were obtained by normalization to DNA quantification data (i.e., results are expressed as pg/mL/ng DNA content).

2.5.4. Macrophage Polarization Assessment. For immunostaining, THP-1 was cultured on the experimental discs for 1, 4, and 7 days. After that, the cells were fixed with 500 μL of 3.7% paraformaldehyde (PFA) for 10 min at room temperature and blocked with 500 μL of 1% bovine serum albumin (BSA) for 15 min. After blocking, the discs were incubated with primary antibodies CCR7 (M1 macrophage marker; Abcam, Cambridge MA, United States) and CD36 (M2 macrophage marker; Biolegend, San Diego CA, United States) overnight at 4 °C. The sections were washed 3 times with PBS, incubated for 1 h with Alexa-Fluor 488 or 568 secondary antibodies, and then incubated with DAPI (nucleus; Thermo Fisher Scientific, Waltham MA, United States) for 5 min. Microscopy images were obtained using a fluorescent microscope equipped with a digital camera (Carl Zeiss, Göttingen, Germany). The exposure time of each light channel was kept the same for all samples. The relative intensity of each fluorescence after images collection was analyzed using ImageJ (U.S. National Institutes of Health, Bethesda, United States). The values of red (Alexa-568) and green (Alexa-488) fluorescence of each sample were further normalized to the value of blue fluorescence (DAPI).

2.5.5. Quantitative PCR. Quantitative PCR (qPCR) was performed to detect the macrophage polarization markers indoleamine 2,3-dioxygenase (INDO) (M1), CXCL11 (M1), MCR-1 (M2), and CCL13 (M2). Total RNA was isolated from the cells using TRIzol reagent (Invitrogen, Darmstadt, Germany) according to the manufacturer's instructions. In brief, after removing the culture medium, 1 mL of TRIzol reagent was added to each well. The cell extract was mixed vigorously with 0.2 mL of chloroform and centrifuged at 12 000g for 15 min at 4 °C. The aqueous phase of the sample was collected and mixed with 0.5 mL of 100% isopropanol. After incubation at room temperature for 10 min, the extract was centrifuged and then washed with 75% ethanol. Successively, the RNA pellet was dissolved in RNase-free water, and concentration and purity was determined using the NanoDrop (ND-2000; Thermo Scientific, Waltham MA, United States).

For real-time PCR, total RNA (1 μg) was applied as template for cDNA synthesis using the iScript cDNA synthesis kit (Bio-Rad, Veenendaal, The Netherlands) following the manufacturer's instructions. The cDNA samples were subjected to quantitative real time polymerase chain reaction (qRT-PCR) using a BIORAD CFX96 real-time system.

Oligonucleotide primers were designed for human β-actin, INDO, CXCL11, MCR-1, and CCL13 (Table 1). All real-time primers were initially tested against standards, and a standard curve was generated. The optimized PCR conditions were: initial denaturation at 94 °C for 10 min, followed by 40 cycles consisting of denaturation at 94 °C for 15 s, annealing at 60 °C for 1 min, and extension at 72 °C for 60 s. Negative control reactions with no template (deionized water) were also included in each run. For each gene, all samples were amplified simultaneously in duplicate in one assay run. Analyses of relative gene

expression were performed using the $2^{-\Delta\Delta CT}$ method. Human β-actin was used as a housekeeping gene to normalize gene expression data.

2.6. Statistical Analysis. Data are presented as mean ± standard deviation of the mean. The normality of all variables was verified using the Shapiro−Wilk W-test. For coating thickness and roughness analysis, Student's t tests were used. For the multiple analyses of variables that exhibited normal distribution (i.e., cytokine secretion and macrophage proliferation, polarization, and gene expression), comparisons among the groups were made using one-way analysis of variance (ANOVA) with a posthoc Tukey multiple comparisons test. For variables that exhibited non-normal distribution (i.e., roughness analysis, coating stability, platelet adhesion, and monocyte/macro-phage proliferation), Kruskal−Wallis tests were used with posthoc Dunn tests. GraphPad Prism version 6.01 (Software Mackiev, Boston, MA, United States) was used to perform statistical analysis. Values of p < 0.05 were considered statistically significant.

3. RESULTS

3.1. Material Preparation and Characterization. *3.1.1. Surface Analysis.* SEM was used to morphologically examine the topography of the different material surfaces. SEM results of Thermanox, grit-blasted Ti, HA, and β-TCP are depicted in Figure 1. Thermanox showed a smooth appearance, whereas grit-blasted Ti, Ti-HA, and Ti-β-TCP exhibited apparent roughness (Figure 1A).
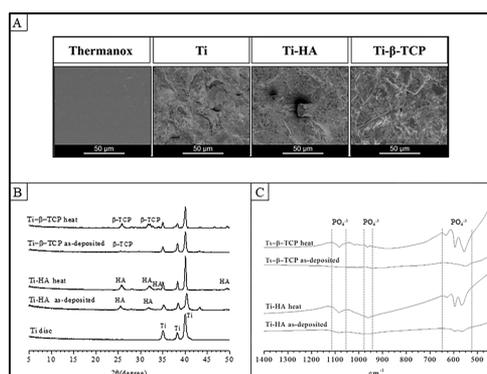

Figure 1. (A) SEM micrographs of Thermanox, grit-blasted Ti, Ti-HA, and Ti-β-TCP surfaces. (B) X-ray diffraction spectra of grit-blasted Ti and as-deposited and heat treated Ti-HA and Ti-β-TCP coatings. (C) Fourier transform infrared spectra of as-deposited and heat treated Ti-HA and Ti-β-TCP.

Table 2 depicts the results of thickness and roughness analyses of grit-blasted Ti, HA, and Ti-β-TCP. The average

Table 2. Coating Thickness and Roughness (Mean ± SD)

experimental group	coating thickness (μm)	roughness (μm)
Thermanox		
grit-blasted Ti		2.598 ± 0.074
Ti-HA	1.423 ± 0.229	2.425 ± 0.049
Ti-β-TCP	1.688 ± 0.130	2.538 ± 0.092

thickness of HA and β-TCP coatings was 1.423 ± 0.229 and 1.688 ± 0.130 μm, respectively (p > 0.05). The roughness of grit-blasted Ti, Ti-HA, and Ti-β-TCP was similar with average R_a values of 2.598 ± 0.074, 2.425 ± 0.049, and 2.538 ± 0.092 μm, respectively (p > 0.05).

3.1.2. Physicochemical Characterization. Figure 1B shows the XRD patterns of grit-blasted Ti, HA, and β-TCP (as-deposited and with heat treatment). The XRD patterns of grit-

blasted Ti showed characteristic titanium peaks at 35.04, 38.40, and 40.10° (ICDD 5-682). The XRD pattern of as-deposited HA showed 2 characteristic peaks at 25.9° and 32° that can be attributed to apatite. The XRD patterns of as-deposited β-TCP presented peaks (26, 32, and 34°) with low intensity. However, heat treatment increased the intensity of peaks in the XRD pattern at 34 and 49° for HA (ICDD 9-0432) and 26, 32, and 34° for β-TCP (ICDD 9-169). These results indicate that heat treatment evoked a more crystalline structure in the ceramic coatings.

These findings were confirmed by FTIR spectra of HA and β-TCP as-deposited and after heat treatment (Figure 1C). HA coating showed bands at 575, 670, 970, 1050, and 1090 cm^{-1} (stretching and bending motion of phosphate).[20] These P−O bonds of calcium phosphate appear sharper after heat treatment. Furthermore, the β-TCP coating spectrum presented bands in the same regions as HA coatings (575, 670, 970, 1050, and 1090 cm^{-1}), characteristic of stretching and bending motion of phosphate.[20] After heat treatment can be observed, sharper bands revealing that this treatment was effective to make the coating more crystalline. Therefore, both spectra showed similar characteristic absorption bands at 500−650 cm^{-1} (P−O bending) and 900−1200 cm^{-1} (P−O stretching), which increased after heat treatment and match with the crystalline structure of HA and β-TCP.

3.2. Coating Stability. Table 3 shows the total amount of calcium on the surface of the coated discs (μg/cm^2). Ti-HA and

Table 3. Total Amount of Calcium per cm^2 on the Discs (Mean ± SD)

discs	total amount of calcium (μg/cm^2)
Ti-HA as-deposited	177.12 ± 14.47
Ti-HA heat	191.67 ± 14.70
Ti-β-TCP as-deposited	186.80 ± 6.82
Ti-β-TCP heat	182.06 ± 24.97

Ti-β-TCP coatings showed similar calcium amounts within the coating of 177.12 ± 14.47 μg/cm^2 (as-deposited Ti-HA), 191.67 ± 14.70 μg/cm^2 (heat-treated Ti-HA), 186.80 ± 6.82 μg/cm^2 (as-deposited Ti-β-TCP), and 182.06 ± 24.97 μg/cm^2 (heat-treated Ti-β-TCP).

Figure 2A presents cumulative calcium release from the Ti-HA and Ti-β-TCP coatings after 7, 14, 21, and 28 days incubation in Milli-Q. Cumulative calcium release was significantly higher for Ti-β-TCP coatings compared to Ti-HA coatings after 7 days (p = 0.036) and after 21 days (p = 0.037). No significant differences between as-deposited and heat treated coatings were observed, irrespective of CaP coating type (p > 0.05).

After 28 days, the calcium remaining on the discs was measured (Figure 2B). Calcium remaining for Ti-HA heat (130.73 μg/cm^2) was higher when compared to Ti-β-TCP heat (58.15 μg/cm^2) (p = 0.011).

3.3. Platelet Experiments. *3.3.1. Platelet Morphology.* Qualitative analyses of platelet adhesion and morphology were performed with SEM (Figure 3A). On Thermanox, numbers of platelets with spherical shape and some platelets with changes in their shape (development of tiny pseudopodia) were observed. On grit-blasted Ti, Ti-HA, and Ti-β-TCP, the platelets were more difficult to identify because of the roughness of the discs. However, on grit-blasted Ti, Ti-HA, and Ti- β-TCP, the appearance of adherent platelets was
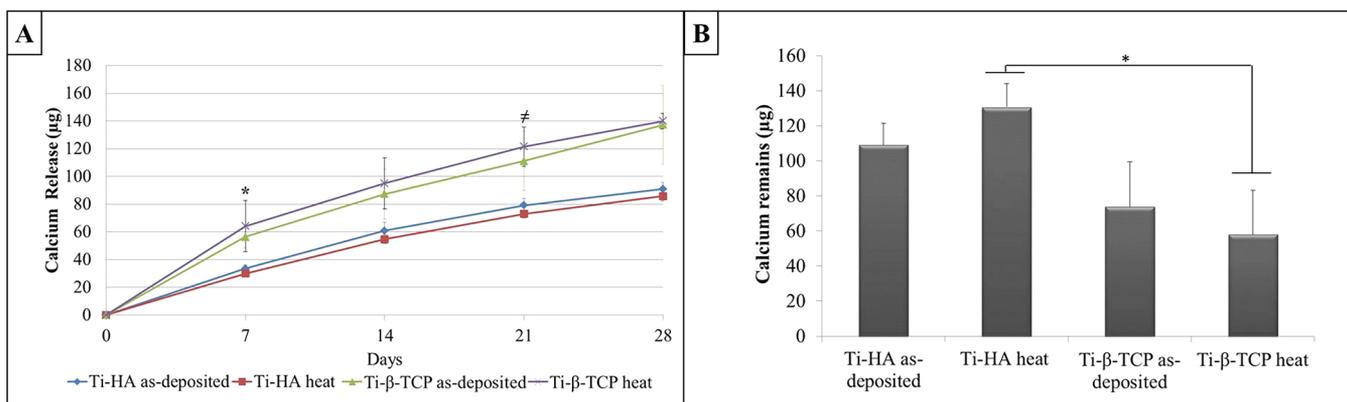
Figure 2. (A) Calcium release from as-deposited and heat-treated Ti-HA and Ti-β-TCP coatings over a 28-day incubation period in Milli-Q water (n = 3). * p = 0.036 Ti-β-TCP heat vs Ti-HA heat; $\neq$ p = 0.037 Ti-β-TCP heat vs Ti-HA heat. (B) Calcium remaining on the coated discs after 28 days in Milli-Q water soaking experiment for as-deposited and heat treated HA and β-TCP coatings (n = 3). Data analysis was performed using Kruskal−Wallis test with a posthoc Dunn test. * p = 0.011.
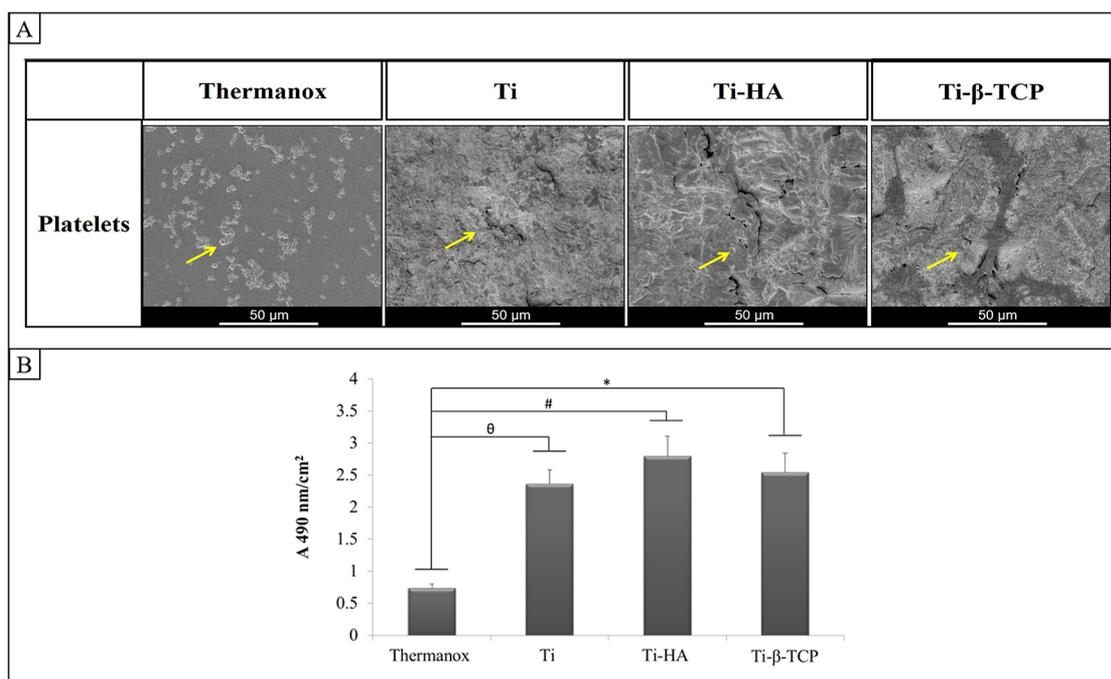

Figure 3. (A) Scanning electron micrograph of platelets on Thermanox, grit-blasted Ti, Ti-HA, and Ti-β-TCP. Yellow arrows indicate the platelets. (B) LDH activity assay for platelets adhered to Thermanox and grit-blasted Ti, Ti-HA, and Ti-β-TCP (n = 4). Data analysis was performed using Kruskal−Wallis test with a posthoc Dunn test. Results represent mean + SD (n = 4). *Thermanox vs Ti-β-TCP (p = 0.00011); # Thermanox vs Ti-HA (p = 0.0007); θ Thermanox vs grit-blasted Ti (p = 0.0024).

similar, showing spherical platelets spread and aggregated on the disc surface.

3.3.2. Platelet Adhesion (LDH Activity Assay). Quantitative analysis of platelet adhesion based on LDH activity assay (Figure 3B) showed a significant increase in platelet adherence to grit-blasted Ti (p = 0.0024), Ti-HA (p = 0.0007), and Ti-β-TCP (p = 0.0011) compared to Thermanox (p = 0.0024, 0.0007, and 0.0011, respectively).

3.4. Macrophage Experiments. *3.4.1. Cell Morphology.* Morphology of macrophages after 1, 4, and 7 days of culture on the different experimental surfaces was observed (Figure 4). Spherical macrophages were observed at the first day on Thermanox. Interestingly, after four and seven days, morphological changes were observed in the form of prolongations. In contrast, macrophages showed a faster transition to a flattened

morphology on rough surfaces of grit-blasted Ti, Ti-HA, and Ti-β-TCP.

3.4.2. Cell Proliferation. The DNA content of macrophages seeded on the different experimental substrates after culture periods of 1, 4, and 7 days are presented in Figure 5A. Both grit-blasted Ti and Thermanox showed an increase in DNA content values from days 1−4 and a decrease thereafter to day 7. In contrast, Ti-HA and Ti-β-TCP showed similar DNA content values over time, both of which were significantly lower compared to those of grit-blasted Ti and Thermanox.

3.4.3. Cytokine Secretion. Secretion levels for the cytokines TNF-α and TGF-β are presented in Figures 5B and C. After 1 day, TNF-α secretion was significantly higher for Ti-β-TCP compared to Thermanox (p = 0.008). After 4 days, Ti-HA showed significantly higher secretion of TNF-α compared to
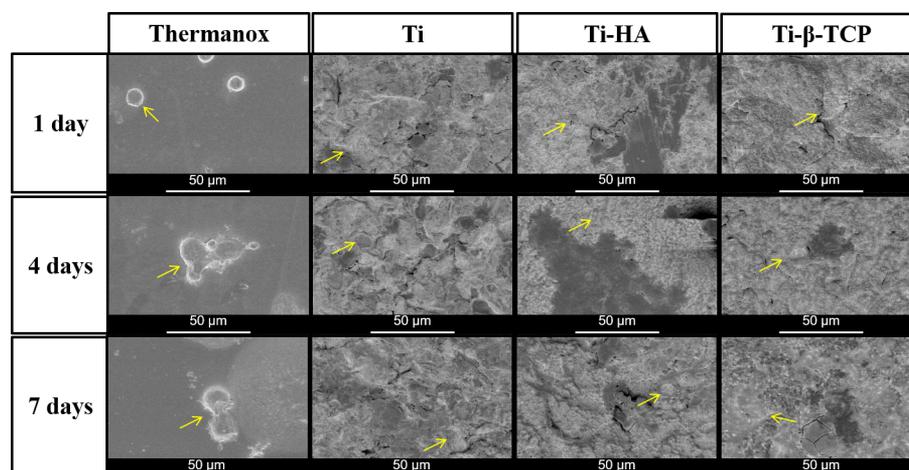
Figure 4. (A) Scanning electron microscopy images of macrophages cultivated on Thermanox and grit-blasted Ti, Ti-HA, and Ti-β-TCP after 1, 4, and 7 days of cultivation. Yellow arrows indicate macrophages (original magnification: 1000×; scale bar: 50 μm).
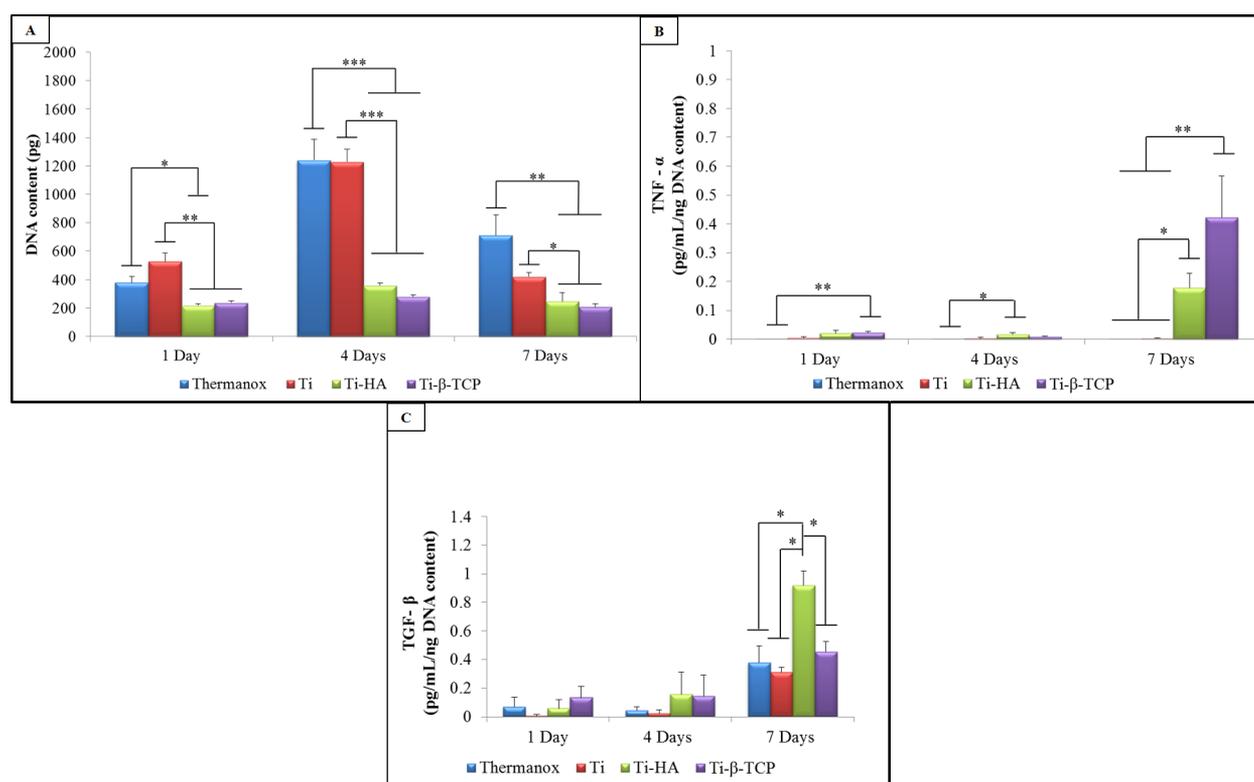

Figure 5. (A) DNA content (ng) of macrophages cultured on Thermanox and grit-blasted Ti, Ti-HA, and Ti-β-TCP. Results represent mean + SD (n = 4). * $p < 0.05$; ** $p < 0.01$; and *** $p < 0.001$. (B) TNF-α and TGF-β (C) secretion of macrophages after 1, 4, and 7 days of culture on Thermanox and grit-blasted Ti, Ti-HA, and Ti-β-TCP. Results represent mean + SD of 4 experimental groups (n = 4). Data analysis was performed using one-way ANOVA with a posthoc Tukey multiple comparisons test. *$p < 0.05$; **$p < 0.01$; and ***$p < 0.0001$.

Thermanox (p = 0.0318). At day 7, both Ti-HA (0.178 pg/mL/ng DNA) and Ti-β-TCP (0.422 pg/mL/ng DNA content) showed an increased TNF-α secretion compared to days 1 and 4. Additionally, in this period, both Ti-HA and Ti-β-TCP showed a significantly higher secretion of TNF-α compared to Thermanox (p = 0.019) and grit-blasted Ti (p = 0.019).

TGF-β levels (Figure 5C) showed no statistically significant differences during the first 4 days of macrophage culture (range: 0.006−0.156 pg/mL/ng DNA content). At day 7, Ti-HA showed a significantly higher secretion of TGF-β levels (0.920 pg/mL/ng DNA content) compared to those of

Thermanox (0.377 pg/mL/ng DNA content) (p = 0.014), grit-blasted Ti (0.313 pg/mL/ng DNA content) (p = 0.011), and Ti-β-TCP (0.456 pg/mL/ng DNA content) (p = 0.046).

3.4.4. Macrophage Polarization on Experimental Surfaces. Representative fluorescent images of the experimental groups at their corresponding time points are shown in Figure 6. The images demonstrated that all surfaces presented the M1 (CCR7) and M2 (CD36) macrophages markers across all time points. The images also suggest that grit-blasted Ti, Ti-HA, and Ti-β-TCP are effective at maintaining the CD36 staining (M2 macrophages) especially after four days.
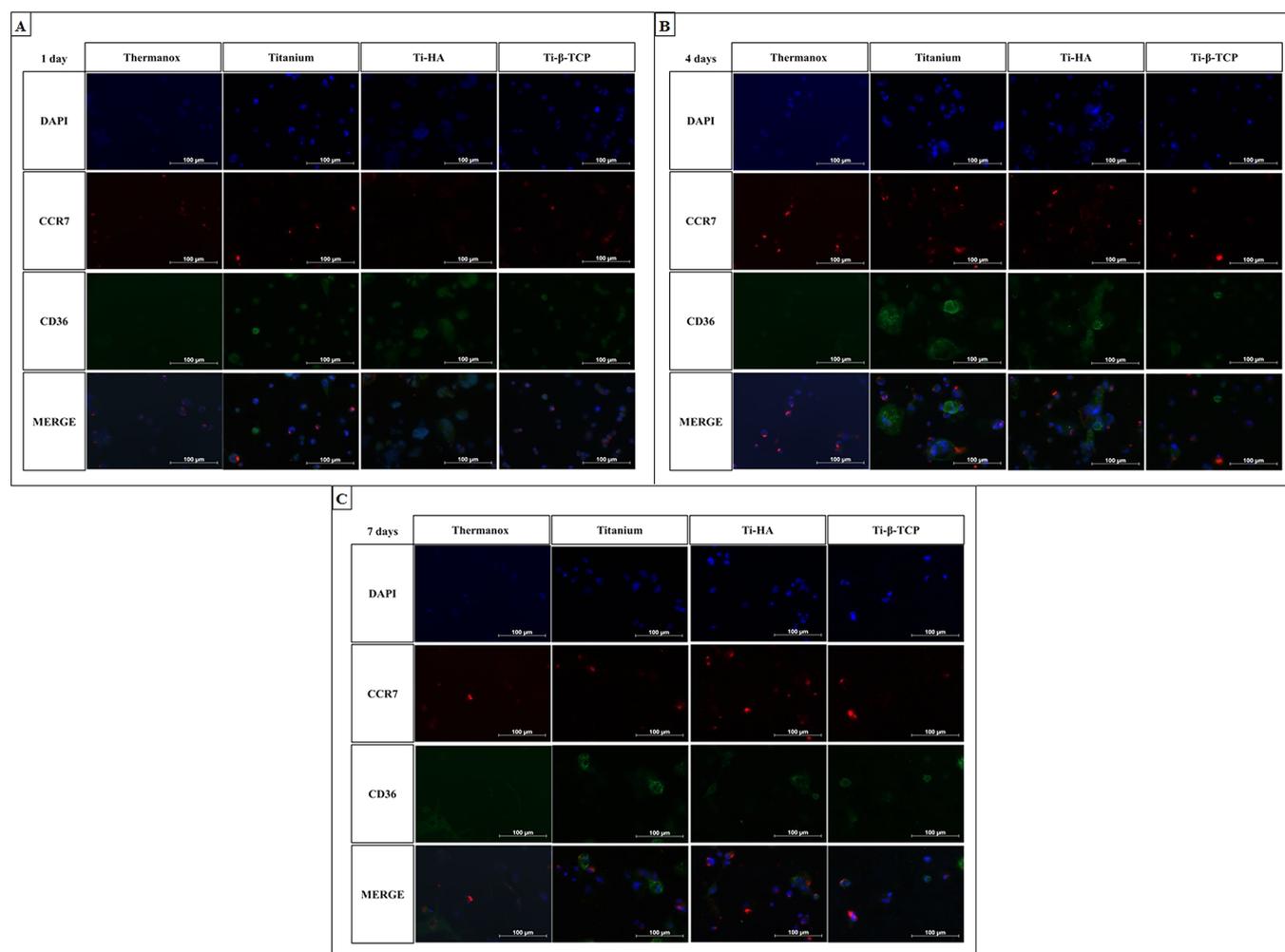
Figure 6. Immunostaining for DAPI (nuclei), CCR7 (M1 marker), CD36 (M2 marker), and merged images for macrophages cultured on grit-blasted Ti, Ti-HA, and Ti-β-TCP discs after cultures of 1 (A), 4 (B), and 7 (C) days.
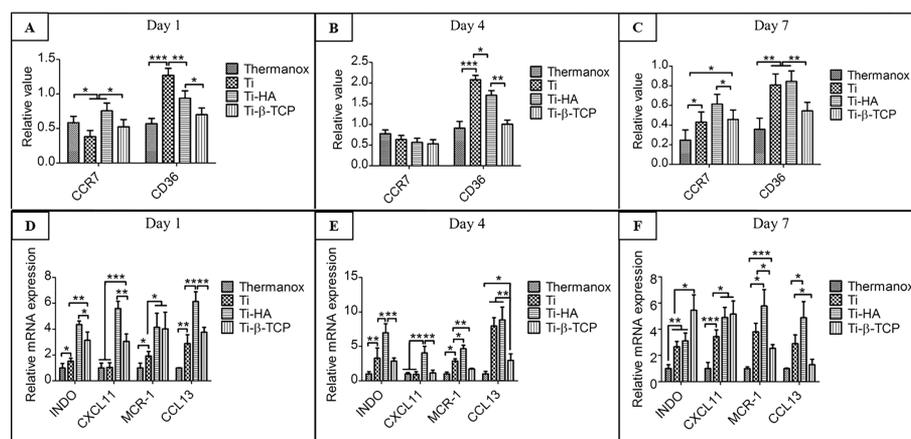

Figure 7. Quantitative immunostaining for CCR7 (M1 marker) and CD36 (M2 marker) for macrophages cultured on Thermanox and grit-blasted Ti, Ti-HA, and Ti-β-TCP discs after cultures of 1 (A), 4 (B), and 7 (C) days ($n = 4$). Quantitative PCR for INDO and CXCL11 (M1 markers) and MCR-1 and CCL13 (M2 markers) for macrophages cultured on Thermanox and grit-blasted Ti, Ti-HA, and Ti-β-TCP discs after cultures of 1 (D), 4 (E), and 7 (F) days ($n = 4$). Data analysis was performed using one-way ANOVA with a posthoc Tukey multiple comparisons test. *$p < 0.05$; **$p < 0.01$; and ***$p < 0.0001$.

Quantification of the immunofluorescent staining was performed. Figures 7A–C show the immunostaining for CCR7 and CD36 after 1, 4, and 7 days. After 1 day, in M1 macrophage marker CCR7 there can be observed a decreased

of labeling in the Ti and an increase in the labeling in the HA (Figure 7A). No significant differences were observed between the Thermanox and Ti-β-TCP in this experimental period. For CD36, an increase in immunostaining was observed in the grit-

blasted Ti, Ti-HA, and Ti-β-TCP compared to Thermanox (Figure 7A). On day 4, no statistically significant difference was observed for CCR7 between the groups analyzed. For CD36, similar results were observed the analysis after one day, with increased immunostaining for CD36 in the Ti, Ti-HA, and Ti-β-TCP groups when compared to that in Thermanox (Figure 7B). Finally, as shown in Figure 7C, CCR7 and CD36 had immunostaining labeling in all groups after 7 days. For CCR7, there can be observed an increase in the Ti-HA compared to that in Thermanox and grit-blasted Ti and Ti-β-TCP. The lowest values for the CCR7 immunostaining were observed in Thermanox. No significant differences were observed between the grit-blasted Ti and Ti-β-TCP in this experimental period. For CD36, the grit-blasted Ti and Ti-HA demonstrated higher values of immunolabeling compared to those in Thermanox and Ti-β-TCP.

3.4.5. Quantitative PCR. The macrophage polarization was also assessed by RT-PCR, in which INDO and CXCL11 were considered as M1 macrophage markers and MCR-1 and CCL13 were considered as M2 macrophage markers. After 1 day, grit-blasted Ti, Ti-HA, and Ti-β-TCP showed more obvious biological activity compared to that of Thermanox controls, which promoted both the M1 macrophage and M2 macrophage polarization process, evidenced by higher INDO, CXCL11, MCR-1, and CCL13 gene expression. Among these, Ti and Ti-HA showed M1 and M2 macrophage marker expression significantly higher than that of β-TCP (Figure 7D). After 4 days, grit-blasted Ti, Ti-HA, and Ti-β-TCP still showed more obvious biological activity compared to Thermanox controls as the trend on day 1. However, the difference is that significantly higher expression of INDO, CXCL11, MCR-1, and CCL13 in the Ti-β-TCP was found compared to grit-blasted Ti. Still, Ti-HA displayed the highest INDO, CXCL11, MCR-1, and CCL13 gene expression in the Ti-HA (Figure 7E).

After 7 days, intriguingly, Ti-β-TCP significantly enhanced the M1 macrophage polarization, evidenced by INDO and CCL11 gene expression and decreased M2 macrophage gene expression MCR-1 and CCL13 compared to Ti-HA and grit-blasted Ti and Thermanox controls (Figure 7F).

4. DISCUSSION

Dental and orthopedic bone implants should provide a complete host tissue integration and moreover prevent an exacerbated immune response. Upon implantation, such biomaterial devices can activate many cells and hence the secretion of cytokines and factors by members of the hematological and immune system.[10−12] This activation is the initial step for bone healing and represents a challenge for the medical field in terms of modulating this foreign body response toward functional performance of implanted biomaterials.[10,14] Here, we evaluated bone implant surface effects on the response of blood-born components that account for the initial biological cascade of events following implantation using in vitro experiments with human platelets and macrophages. The characterization of the different coatings showed that the heat treatment was effective in increasing coating crystallinity but not coating stability. For platelets, higher numbers of adherent platelets were observed for grit-blasted Ti, Ti-HA, and Ti-β-TCP compared to Thermanox. Macrophage experiments showed decreased cell proliferation on CaP-coated Ti-discs (Ti-HA and Ti-β-TCP) compared to that in Thermanox and grit-blasted Ti. However, the coated CaP seems more biological active than Thermanox, proved by upregulated pro-inflamma-

tory and anti-inflammatory cytokine secretion, M1/M2 macrophage marker, and M1/M2 macrophage gene expression. Additionally, Ti-β-TCP demonstrated a more pro-inflammatory function than Ti-HA.

In this study, two calcium phosphate ceramics (CaPs) were used as a coating, the HA and β-TCP. These coatings are considered a class of bioactive materials, which have properties that affect the adhesion and proliferation of immune and bone cells and induce bone formation.[8,20] HA is an osteoconductive biomaterial similar to natural bone mineral both from a chemical and a structural point of view.[35,36] In contrast, β-TCP is a biomaterial used in biomedical applications mainly due to its mechanical performance, chemical stability, solubility, and reabsorption rate.[20,36] These CaP biomaterials were used to provide the Ti discs with a thin coating deposition using the RF sputtering, which has been shown to be useful to control ceramic coating properties and the adhesion between the substrate and the coating[30,37,38] in addition to permitting uniform and continuous deposition coatings.[20,27] After the sputtering, the discs were heat treated in an infrared furnace. This treatment is a necessary postannealing treatment to crystallize the coating. Yoshinari et al.[30] demonstrated that the heat treatment with infrared radiation around 600° was the best treatment for RF magnetron sputtered coatings, which was used in this study.[30] The physicochemical characterization analyzed by XRD and FTIR of the CaP coatings used in this study showed that the heat treatment was able to increase the crystallinity of the coatings. The physicochemical characteristics of CaPs coatings and their link with the Ti discs is crucial for the first host body response and can affect the success of the implantation. Many studies on bone implants, however, neglect the importance of physicochemical characteristics such as dissolution, crystallinity, and corrosion, among others, and how they alter the microenvironment around the implant.

Platelets play an active role in the immunological and inflammatory aspect of tissue healing in normal hemostasis as well as in host defense. Platelets can be directly involved in the inflammatory response by the production and release of several inflammatory mediators, including a variety of cytokines and chemokines. Furthermore, the ion and/or particle release as calcium release can affect the behavior of the platelets and macrophages.[7] In this study, the calcium assay showed that the β-TCP coatings can permit more calcium release and transform the microenvironment around the implant. It is known that the release of calcium ions plays an essential role in several steps of the bone repair process from platelet activation to biomineralization and bone remodeling.[39] In the process of osseointegration of implants, calcium establishes electrostatic bridges between the surface of the implant and several proteins, modifying them and allowing a better integration of the bone tissue with the implant. In addition, after implantation, the platelets need to be activated to perform their functions properly.[40] In this context, calcium participates in the binding of platelet membrane phospholipids to Factor Xa and Factor IXa, which are necessary for the tenase and prothrombinase complexes that convert prothrombin to thrombin (Factor IIa), polymerizing fibrin.[39,40] Thus, calcium actively participates in platelet adherence and activation and exocytosis of their granules to perform its function. In addition, platelets secrete cytokines, generated from platelets in contact especially with calcium ions (Ca) in the surface can upregulate neutrophil activation and consequently stimulate osteogenic cell proliferation in vivo.[7] Kikuchi et al.[7] observed that the Ca and

phosphate (PO_4^-) in the coatings surface can increase the microtopographical complexity, resulting in an increase in the platelet activation levels. The findings of this work demonstrated that there was no significant difference between Ti-HA and Ti-β-TCP groups on platelet adherence in the discs. It is known that platelet adherence and activation generally occur at the same time when in contact with materials and are closely combined. Additionally, platelet activation results in stimulation and behavior of various leukocytes, including macrophages.[15]

Beside platelets, the other important immune cells in addition to macrophages that migrate to the local implantation site and produce many chemokines, cytokines and growth factors to play an important tissue remodeling response after an injury or in host defense.

In the present study, a significant decrease in the DNA content of macrophages when in contact with CaP coated discs was observed. Besides macrophage adhesion, macrophage polarization has been proved to play crucial roles in bone–implant interaction and further its osseointegration.[41]

Therefore, we investigated effects of different surface chemical properties on macrophage polarization by assessing M1/M2 macrophage cytokine secretion and marker gene expression based on our previous work.[42] We demonstrated a significantly upregulated pro-inflammatory and anti-inflammatory cytokine secretion and marker gene expression of macrophages on HA and β-TCP coatings. This hybrid macrophage phenotype with simultaneous M1 and M2 markers was also reported in previous data.[13] However, its mode of action and functions in in vivo performance remain to be decoded. Furthermore, HA induced an earlier M1 macrophage polarization than β-TCP because M1 macrophage markers CCR7 and CXCL11 and CCR7 immunostaining showed expression higher than those on β-TCP after 1 and 4 days. During this time period, M2 macrophage polarization was also enhanced on HA coated discs. However, after 7 days, β-TCP showed M1 macrophage polarization more obvious than that in HA. These results can be attributed to the overphysiological calcium content in the medium. From the clinical review, HA coating is superior to β-TCP because it is more bioactive, and macrophages around HA will be converted into M2 macrophages after 7 days, which is beneficial for the ending of inflammation and tissue remodeling.

5. CONCLUSION

This study demonstrated that the biomaterial surface property of HA and β-TCP coatings induced different responses to blood-born components that account for the initial biological cascade of events following implantation. Grit-blasted Ti, Ti-HA, and Ti-β-TCP did not display significant differences for platelet adhesion. However, for macrophages, both types of coatings (Ti-HA and Ti-β-TCP) decreased macrophage proliferation more than twice compared to grit-blasted Ti. Furthermore, Ti-β-TCP significantly upregulated pro-inflammatory cytokine TNF-α secretion, while Ti-HA significantly upregulated anti-inflammatory cytokine TGF-β secretion after 7 days of macrophage culture on these surfaces. Immunostaining and gene expression of M1/M2 macrophages further revealed a hybrid macrophage phenotype with simultaneous M1 and M2 markers induced by Ti-HA and Ti-β-TCP compared to grit-blasted Ti. In addition, Ti-HA induced an earlier M1 macrophage polarization and earlier M1-M2 macrophage transformation compared to Ti-TCP. Further studies are required to verify the clinical significance of our findings and

evaluate effects of biomaterial surface properties on multiple cell types in suitable in vitro coculture models and in vivo models with appropriate postimplantation time points.

■ AUTHOR INFORMATION

Corresponding Author
*Tel.: +31 24 366 7305; Fax: +31 24 361 4657; E-mail: jeroen.vandenbeucken@radboudumc.nl.

ORCID
Kelly R. Fernandes: 0000-0003-2851-6896

Author Contributions
§K.R.F. and Y.Z. contributed equally.

Notes
The authors declare no competing financial interest.

■ REFERENCES

(1) Liu, X.; Guan, Y.; Ma, Z.; Liu, H. Surface modification and characterization of magnetic polymer nanospheres prepared by miniemulsion polymerization. *Langmuir* **2004**, *20* (23), 10278–82.

(2) Han, H. J.; Kim, S.; Han, D. H. Multifactorial evaluation of implant failure: a 19-year retrospective study. *International journal of oral & maxillofacial implants* **2014**, *29* (2), 303–10.

(3) Wu, C.; Chen, Z.; Yi, D.; Chang, J.; Xiao, Y. Multidirectional effects of Sr-, Mg-, and Si-containing bioceramic coatings with high bonding strength on inflammation, osteoclastogenesis, and osteogenesis. *ACS Appl. Mater. Interfaces* **2014**, *6* (6), 4264–76.

(4) Rentsch, C.; Rentsch, B.; Heinemann, S.; Bernhardt, R.; Bischoff, B.; Forster, Y.; Scharnweber, D.; Rammelt, S. ECM inspired coating of embroidered 3D scaffolds enhances calvaria bone regeneration. *BioMed Res. Int.* **2014**, *2014*, 217078.

(5) Smieszek, A.; Donesz-Sikorska, A.; Grzesiak, J.; Krzak, J.; Marycz, K. Biological effects of sol-gel derived ZrO2 and SiO2/ZrO2 coatings on stainless steel surface—In vitro model using mesenchymal stem cells. *J. Biomater. Appl.* **2014**, *29* (5), 699–714.

(6) van Oirschot, B. A.; Bronkhorst, E. M.; van den Beucken, J. J.; Meijer, G. J.; Jansen, J. A.; Junker, R. A systematic review on the long-term success of calcium phosphate plasma-spray-coated dental implants. *Odontology* **2016**, *104* (3), 347–56.

(7) Kikuchi, L.; Park, J. Y.; Victor, C.; Davies, J. E. Platelet interactions with calcium-phosphate-coated surfaces. *Biomaterials* **2005**, *26* (26), 5285–95.

(8) Samavedi, S.; Whittington, A. R.; Goldstein, A. S. Calcium phosphate ceramics in bone tissue engineering: a review of properties and their influence on cell behavior. *Acta Biomater.* **2013**, *9* (9), 8037–45.

(9) Kuang, G. M.; Yau, W. P.; Wu, J.; Yeung, K. W.; Pan, H.; Lam, W. M.; Lu, W. W.; Chiu, K. Y. Strontium exerts dual effects on calcium phosphate cement: Accelerating the degradation and enhancing the osteoconductivity both in vitro and in vivo. *J. Biomed. Mater. Res., Part A* **2015**, *103* (5), 1613–21.

(10) Anderson, J. M.; Rodriguez, A.; Chang, D. T. Foreign body reaction to biomaterials. *Semin. Immunol.* **2008**, *20* (2), 86–100.

(11) Kim, Y. H.; Furuya, H.; Tabata, Y. Enhancement of bone regeneration by dual release of a macrophage recruitment agent and platelet-rich plasma from gelatin hydrogels. *Biomaterials* **2014**, *35* (1), 214–24.

(12) Zaveri, T. D.; Lewis, J. S.; Dolgova, N. V.; Clare-Salzler, M. J.; Keselowsky, B. G. Integrin-directed modulation of macrophage responses to biomaterials. *Biomaterials* **2014**, *35* (11), 3504–15.

(13) Lee, C. H.; Kim, Y. J.; Jang, J. H.; Park, J. W. Modulating macrophage polarization with divalent cations in nanostructured titanium implant surfaces. *Nanotechnology* **2016**, *27* (8), 085101.

(14) Chen, Z.; Mao, X.; Tan, L.; Friis, T.; Wu, C.; Crawford, R.; Xiao, Y. Osteoimmunomodulatory properties of magnesium scaffolds coated with beta-tricalcium phosphate. *Biomaterials* **2014**, *35* (30), 8553−65.

(15) Galliera, E.; Corsi, M. M.; Banfi, G. Platelet rich plasma therapy: inflammatory molecules involved in tissue healing. *Journal of biological regulators and homeostatic agents* **2012**, *26* (2 Suppl 1), 35S−42S.

(16) Mantovani, A.; Biswas, S. K.; Galdiero, M. R.; Sica, A.; Locati, M. Macrophage plasticity and polarization in tissue repair and remodelling. *Journal of pathology* **2013**, *229* (2), 176−85.

(17) Martinez, F. O.; Sica, A.; Mantovani, A.; Locati, M. Macrophage activation and polarization. *Front. Biosci., Landmark Ed.* **2008**, *13*, 453−61.

(18) Biswas, S. K.; Mantovani, A. Orchestration of metabolism by macrophages. *Cell Metab.* **2012**, *15* (4), 432−7.

(19) Cochis, A.; Azzimonti, B.; Della Valle, C.; Chiesa, R.; Arciola, C. R.; Rimondini, L. Biofilm formation on titanium implants counteracted by grafting gallium and silver ions. *J. Biomed. Mater. Res., Part A* **2015**, *103* (3), 1176−87.

(20) Urquia Edreira, E. R.; Wolke, J. G.; Aldosari, A. A.; Al-Johany, S. S.; Anil, S.; Jansen, J. A.; van den Beucken, J. J., Effects of calcium phosphate composition in sputter coatings on in vitro and in vivo performance. *J. Biomed. Mater. Res., Part A* **2015**, *103* (1), 300−10.

(21) Popkov, A. V.; Gorbach, E. N.; Kononovich, N. A.; Popkov, D. A.; Tverdokhlebov, S. I.; Shesterikov, E. V. Bioactivity and osteointegration of hydroxyapatite-coated stainless steel and titanium wires used for intramedullary osteosynthesis. *Strategies in trauma and limb reconstruction* **2017**, *12* (2), 107−113.

(22) Fujibayashi, S.; Neo, M.; Kim, H. M.; Kokubo, T.; Nakamura, T. Osteoinduction of porous bioactive titanium metal. *Biomaterials* **2004**, *25* (3), 443−50.

(23) Zweymuller, K. A. [Bony ongrowth on the surface of HA-coated femoral implants: an x-ray analysis]. *Zeitschrift fur Orthopadie und Unfallchirurgie* **2012**, *150* (1), 27−31.

(24) Onodera, J.; Kondo, E.; Omizu, N.; Ueda, D.; Yagi, T.; Yasuda, K. Beta-tricalcium phosphate shows superior absorption rate and osteoconductivity compared to hydroxyapatite in open-wedge high tibial osteotomy. *Knee surgery, sports traumatology, arthroscopy: official journal of the ESSKA* **2014**, *22* (11), 2763−70.

(25) Oh, K. J.; Ko, Y. B.; Jaiswal, S.; Whang, I. C. Comparison of osteoconductivity and absorbability of beta-tricalcium phosphate and hydroxyapatite in clinical scenario of opening wedge high tibial osteotomy. *J. Mater. Sci.: Mater. Med.* **2016**, *27* (12), 179.

(26) Shariff, K. A.; Tsuru, K.; Ishikawa, K. Fabrication of dicalcium phosphate dihydrate-coated beta-TCP granules and evaluation of their osteoconductivity using experimental rats. *Mater. Sci. Eng., C* **2017**, *75*, 1411−1419.

(27) Wolke, J. G.; van Dijk, K.; Schaeken, H. G.; de Groot, K.; Jansen, J. A. Study of the surface characteristics of magnetron-sputter calcium phosphate coatings. *J. Biomed. Mater. Res.* **1994**, *28* (12), 1477−84.

(28) Jansen, J. A.; Wolke, J. G.; Swann, S.; Van der Waerden, J. P.; de Groof, K. Application of magnetron sputtering for producing ceramic coatings on implant materials. *Clinical oral implants research* **1993**, *4* (1), 28−34.

(29) Shi, L.; Peng, X.; Ahmed, M. A.; Edwards, D.; Brown, L. S.; Ladizhansky, V. Resolution enhancement by homonuclear J-decoupling: application to three-dimensional solid-state magic angle spinning NMR spectroscopy. *J. Biomol. NMR* **2008**, *41* (1), 9−15.

(30) Yoshinari, M.; Hayakawa, T.; Wolke, J. G.; Nemoto, K.; Jansen, J. A. Influence of rapid heating with infrared radiation on RF magnetron-sputtered calcium phosphate coatings. *J. Biomed. Mater. Res.* **1997**, *37* (1), 60−7.

(31) Siebers, M. C.; Walboomers, X. F.; Leeuwenburgh, S. C.; Wolke, J. G.; Jansen, J. A. Electrostatic spray deposition (ESD) of calcium phosphate coatings, an in vitro study with osteoblast-like cells. *Biomaterials* **2004**, *25* (11), 2019−27.

(32) Tamada, Y.; Kulik, E. A.; Ikada, Y. Simple method for platelet counting. *Biomaterials* **1995**, *16* (3), 259−61.

(33) Park, J. Y.; Gemmell, C. H.; Davies, J. E. Platelet interactions with titanium: modulation of platelet activity by surface topography. *Biomaterials* **2001**, *22* (19), 2671−82.

(34) Lund, M. E.; To, J.; O'Brien, B. A.; Donnelly, S. The choice of phorbol 12-myristate 13-acetate differentiation protocol influences the response of THP-1 macrophages to a pro-inflammatory stimulus. *J. Immunol. Methods* **2016**, *430*, 64−70.

(35) Jin, S. D.; Um, S. C.; Lee, J. K. Surface Modification of Zirconia Substrate by Calcium Phosphate Particles Using Sol-Gel Method. *J. Nanosci. Nanotechnol.* **2015**, *15* (8), 5946−50.

(36) Bellucci, D.; Sola, A.; Cannillo, V. Hydroxyapatite and tricalcium phosphate composites with bioactive glass as second phase: State of the art and current applications. *J. Biomed. Mater. Res., Part A* **2016**, *104* (4), 1030−56.

(37) Boyd, A. R.; Burke, G. A.; Duffy, H.; Holmberg, M.; O'Kane, C.; Meenan, B. J.; Kingshott, P. Sputter deposited bioceramic coatings: surface characterisation and initial protein adsorption studies using surface-MALDI-MS. *J. Mater. Sci.: Mater. Med.* **2011**, *22* (1), 71−84.

(38) Boyd, A. R.; Rutledge, L.; Randolph, L. D.; Meenan, B. J. Strontium-substituted hydroxyapatite coatings deposited via a co-deposition sputter technique. *Mater. Sci. Eng., C* **2015**, *46*, 290−300.

(39) Anitua, E.; Prado, R.; Orive, G.; Tejero, R. Effects of calcium-modified titanium implant surfaces on platelet activation, clot formation, and osseointegration. *J. Biomed. Mater. Res., Part A* **2015**, *103* (3), 969−80.

(40) Gupta, S.; Reviakine, I. Platelet activation profiles on TiO2: effect of Ca2+ binding to the surface. *Biointerphases* **2012**, *7* (1−4), 28.

(41) Ma, Q. L.; Zhao, L. Z.; Liu, R. R.; Jin, B. Q.; Song, W.; Wang, Y.; Zhang, Y. S.; Chen, L. H.; Zhang, Y. M. Improved implant osseointegration of a nanostructured titanium surface via mediation of macrophage polarization. *Biomaterials* **2014**, *35* (37), 9853−67.

(42) Zhang, Y.; Bose, T.; Unger, R. E.; Jansen, J. A.; Kirkpatrick, C. J.; van den Beucken, J. J. Macrophage type modulates osteogenic differentiation of adipose tissue MSCs. *Cell Tissue Res.* **2017**, *369*, 273.